RSC Advances

This article can be cited before page numbers have been issued, to do this please use: M. Zhang, Y. Li, D. Pan, Z. Yan, S. Meng and J. Xie, *RSC Adv.*, 2016, DOI: 10.1039/C6RA06416G.

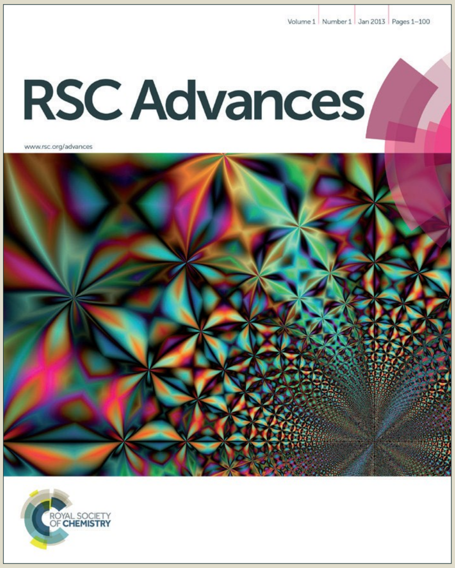

ROYAL SOCIETY
OF CHEMISTRY

www.rsc.org/advances

View Article Online
DOI: 10.1039/C6RA06416G

Nickel core-Palladium shell nanoparticles growing on nitrogen-doped graphene with enhanced electrocatalytic performance for ethanol oxidation

Mingmei Zhang*, Yuan Li, Denghui Pan, Zaoxue Yan, Suci Meng, Jimin Xie
School of Chemistry and Chemical Engineering, Jiangsu University, Zhenjiang 212013, P. R. China

Abstract

Here we report a facile two-step strategy for green synthesis of nickel core-palladium shell nanoclusters on nitrogen-doped graphene (Ni@Pd/NG) without any surfactant and additional reducing agent. During the synthesis, nitrogen-doped graphene acts as both the active substance and support by taking advantage of its moderate reducing and highly dispersing capacities. Characterization indicated that a uniform dispersion of Ni@Pd nanoparticles on nitrogen-doped reduced graphene oxide have the average particle size of 2.8 nm. Unexpectedly, the as-prepared Ni@Pd/NG hybrid exhibits much greater activity and stability than that of Pd/graphene and commercial Pd/C electrocatalyst at the same Pd loadings. Possible mechanisms for the enhanced electrocatalytic performance of nitrogen-doped reduced graphene oxide after combining with Ni@Pd were proposed. The present study provides an efficient strategy to synthesize highly efficient electrocatalyst.

Key words: nitrogen-doped graphene; core/shell nanoelectrocatalyst; alcohol

---

* Correspondence author Tel: +86 11 88791708; fax: +86 11 88791800.
E-mail address: jdzmm@163.com

View Article Online
DOI: 10.1039/C6RA06416G

oxidation; fuel cell

1. Introduction

Among all types of fuel cells, direct ethanol fuel cells (DEFCs) based on liquid fuels is a promising biomass-derived power sources and widely investigated due to its unique properties including higher theoretical mass energy density, lower toxicity and operating temperature, easier in handling and transportation than other types of fuel cells [1-3]. Moreover, ethanol can be easily obtained on a large scale from chemical industry and fermentation of agricultural products or biomass [4].In the development of DEFCs technology, the highly active electro-catalysts are important and necessary in order to completely oxidize each ethanol. Therefore, it has become a hot topic research to design and develop efficient ethanol electro-oxidation anode catalysts for DEFCs, especially in alkaline media[5]. Nowadays, the electrocatalysts of anode catalyst in DEFCs have predominantly relied on Pt based catalysts which have been extensively investigated [6-9]. Nevertheless, the high cost has been remaining the choke point in the popular application of fuel cells for a long time, especially the high cost of the noble metal supported electrocatalyst, which is one of the most critical units in fuel cell systems. It is necessary to develop new catalyst materials or improve the efficiency of existing catalysts and supports for alcohol oxidation. Thus, there is a strong motivation to increase the utilization of catalysts via their dispersion as small particles on a support material. Recently, Pd-based nano-electrocatalysts are emerging

View Article Online
DOI: 10.1039/C6RA06416G

as excellent substitute to Pt-based catalysts and have been proved to be a promising candidate for direct ethanol fuel cells because of more abundance, much cheaper, higher electrocatalytic activity and greater resistance to intermediate products for ethanol electro-oxidation in alkaline medium[10]. However, there are also a number of challenges and obstacles for Pd based nano-electrocatalysts, such as low utilization efficiency of Pd, which hinder the practical application in commercialization of portable fuel cell technology. Till today, it is still necessary to develop low-cost, effective catalysts for DEFCs. Noticeably, most noble metal NPs catalytic reactions occur only on the surface of the NPs and a large fraction of atoms in the core are catalytically inactive. Therefore, to make a large percentage of noble metal atoms available for catalysis and to reduce their consumption, the inner noble metal atoms should be replaced by other non-noble metals[11-12]. A variety of core-shell nanoparticles have also been reported as catalysts in DMFCs. Density functional theory studies suggested that the enhanced catalytic activity for the core-shell nanoparticle originates from a combination of an increased availability of CO-free Pt surface sites on the Ru@Pt nanoparticles and a hydrogen-mediated low-temperature CO oxidation process that is clearly distinct from the traditional bifunctional CO oxidation mechanism[13]. Currently, more research focus on the core/shell structure with noble metal as shell and base transition metal (Ni、Co 、Cu、Fe) as core[14-16]. Consequently, a noble metal at outer surface and base metal second atomic layer instead of noble metal as electrocatalyst promoters changes the catalytic activity, selectivity, and stability owing to synergistic effects[17]. Besides the active metal regulation, another alternative effective approach to enhance electrocatalytic activity is to seek and develop novel catalyst support[18-20]. Graphene, as an atomic-layer-thick two dimensional material, displays intriguing potential benefit as a support material for DEFCs due to its many unique chemical and physical properties such as superior electrical conductivity, high surface-to-volume ratio, ultrathin thickness, structural flexibility and chemical stability [21-23]. Recently, heteroatom doped graphene materials have received much attention as support for electrocatalysts, paving the way for the growth of catalytically active metals with controlled morphology and dispersion on the surface of graphene support [24-25]. To further tailor the catalytic support properties of graphene, the nitrogen doping is important and perhaps the most frequently chosen method which can enhance the conductivity of graphene and induces n-type semi-conductor behavior, because of the nitrogen atom is of comparable atomic size and contains five valence electrons available to form strong valence bonds with carbon atoms [26, 27]. More importantly, the nitrogen-doped graphene (NG) with more functional groups for property design would be provided by the incorporating different types of nitrogen into the carbon network of graphene [28, 29]. Recent studies show that nitrogen doping of catalyst supporting materials can provide small particle sizes and a high dispersion of the catalyst nanoparticles, strong bonding between the support and catalyst, electronic structure modification of the catalysts and an increase in the electronic conductivity of the supports. In addition, studies also show that, nitrogen doped graphene can act as good electrocatalysts even in the absence of precious metals [30]. Inspired by our previous studies, it is of great interest to develop

View Article Online
DOI: 10.1039/C6RA06416G

highly active Ni_{core}–Pd_{shell} supported on N doped-graphene catalysts for the ethanol oxidation reaction. Since metal nano-particles interact strongly with the nitrogen-doped graphene surface, it can highly be dispersed and show good stability with the graphene surface, and the interaction between Ni core and Pd shell which make Ni@Pd/NG setting up a fairly conductive network to facile charge-transfer and mass-transfer processes. Therefore, the combination of Ni@Pd nanoparticles (NPs) and NG may open up a new avenue for designing the next generation catalysts for DEFCs.

In this article, Ni@Pd core/shell nanoparticles supported on nitrogen-doped graphene (Ni@Pd/NG) and its electrocatalytic activity and stability for alcohol oxidation were presented. The preparation of Ni@Pd core/shell nanostructure could not only reduce the consumption of Pd, but also take advantage of the interaction between Ni core and Pd shell such as the ligand effect, downshift in d-band energy center which are favourable for the promotion of the electrochemical activity and stability of Ni@Pd/NG nanostructure[31]. At the same time, N-doped graphene not only serve as support, but also act as a secondary catalyst, which could increase the accessibility of the active sites. The immobilization of Ni@Pd NPs embed on the N doped graphene to fabricate the Ni@Pd/NG nanocatalyst would be promising for the purpose of preventing the aggregation of Ni@Pd. We applied the Ni@Pd/NG to catalyzing alcohol oxidation, where the possible origin of the large surface area and excellent chemical stability of Ni@Pd/ NG was discussed.

View Article Online
DOI: 10.1039/C6RA06416G

2. Experimental details

2.1. Materials

Natural flake graphite was obtained from Qingdao Guyu graphite Co., Ltd. with a particle size of 150 nm. Nickel acetate tetrahydrate ($Ni(ac)_2$ •$4H_2O$), Ethylene glycol, ammonia and Palladium chloride ($PdCl_2$) were purchased from Sinopharm Chemical Reagent Co., Ltd., China and used as received without any further purification. Distilled water was also used throughout the experiment.

2.2. Synthesis of GO and NRGO

Graphite oxide (GO) was prepared from purified natural graphite using a modified Hummers' method [32]. A mixture of 3.0 g of graphite powder, 150 mL of H_2SO_4 and 6.0 g of $NaNO_3$ was prepared and immersed into ice bath. Then, $KMnO_4$ (8.0 g) were added gradually under stirring and the temperature of the mixture was maintained below 10◦C. After stabilization of the reaction temperature, the reaction media was heated at 80°C and stirred for 2h until it became pasty brownish, and then diluted with distilled water. Successively, the mixture was stirred for 30 min and 25 mL of 30 wt. % H_2O_2 solution was slowly added to the mixture to reduce the residual $KMnO_4$, after which the color of the mixture changed to brilliant yellow. The solid product was separated by centrifugation and washed repeatedly with 5% HCl solution to remove metal ions followed by 1.5 L of distilled water to remove the acid. For further purification, the resulting solid was re-dispersed in distilled water and dialyzed for one week to remove any residual salts and acids. Finally, the solid was separated

View Article Online
DOI: 10.1039/C6RA06416G

by sintered discs and freeze-dried.

To synthesize NRGO material, 80 mg of GO were dispersed into 60 mL water and magnetically stirred for 3 h. GO was exfoliated by sonication for 2 h. After that, certain amount of urea was also added in and the solution was ultrasonicated for another 0.5 h. Finally, the mixture was transferred into a 50 mL Teflon lined stainless steel autoclave and was heated at 180°C for 12 h. The resulting product was filtered, washed with distilled water for several times and freeze-dried.

2.3 Preparation of Ni/ NG composite

For synthesizing the Ni/ NG compounds, 25 mg of NRGO was dispersed in 100 mL of ethylene glycol (EG) by sonication for 60 min. Then the solution was added with 15 mg of Nickel acetate under vigorously stirring, and then subjected to microwave (MW) oven (900 W) for intermittent microwave heating at a 20 s on and 10 s off procedure for 15 times in a microwave oven temperature 180 °C. The pH of the entire solution was adjusted to 10 by adding NaOH (2.0 M). After cooling to room temperature, the product was washed with distilled water for 5-6 times to remove the excess EG and subsequent separation by sintered discs and dried in vacuum at 80 °C for 24 h. Finally the nickel impregnated nitrogen-doped graphene (Ni/NG) was obtained. The Ni contents of were analyzed by inductively coupled plasma spectroscopy (ICP, Optima2000DV, USA) analysis, which showed 26.5 wt. % of Ni in Ni/NG compound.

2.4 Preparation of Ni@Pd/ NG electrocatalyst

Ni@Pd/NG nanosized electrocatalysts were synthesized using replacement

View Article Online
DOI: 10.1039/C6RA06416G

method. Typically, 20 mL of 0.093 mol/L H_2PdCl_4 and 1.65 g Ni/NG were dispersed in 50mL distilled water in beaker. The resulting solution was uniformly dispersed by sonification for 10 min, and then vigorously stirred for 24 h at room temperature. So that spontaneous Ni replacement by Pd occurred:

$$2Ni/NG + PdCl_4^{2-} \rightarrow Pd(Ni)/NG + 2Ni^{2+} + 6Cl^-$$

These reactions are thermodynamically favorable since the standard potentials of the Ni^{2+}/Ni couples are -0.257 V vs. SHE, they are lower than the standard potential of the Pd (II) Cl_4^{2-}/Pd couple (+0.951 V vs. SHE). The black solid was separated by sintered discs, washed with deioned water for several times, and finally dried in a vacuum oven at 60 °C. For comparison, Pd nanoparticles supported on nitrogen-doped reduced graphene oxide (Pd/NG) as electrocatalyst was also obtained directly by reducing the H_2PdCl_4 in graphene suspension using ethylene glycol microwave reduction. The theoretical Pd contents in both Ni@Pd/ NG and Pd/ NG were targeted at 15 wt. %. The ICP analysis gave the actual Pd contents as 13.8wt. % for Ni@Pd/ NG and 13.5 wt. % for Pd/ NG, respectively.

2.5 Preparation of catalyst electrode

For electrode preparation, 25.1 mg Ni@Pd/NG were dispersed in 1 mL ethanol and 1 mL 0.5 wt. % Nafion suspension (DuPont, USA) under ultrasonic agitation to form the electrocatalyst ink. The electrocatalyst ink (40 μL) was then deposited on the surface of the glassy carbon rod and dried at room temperature overnight. The total Pd loadings were controlled at 0.02 mg cm^{-2}. All chemicals were of analytical grade and used as received.

View Article Online
DOI: 10.1039/C6RA06416G

2.6 Characterization of the supports and the electrocatalysts

The particle sizes and shapes of the as-prepared samples were examined by a transmission electron microscopy (TEM, JEOL-JEM-2010, Japan) operating at 200 kV. The as-synthesized products were washed with absolute ethyl alcohol to remove impurities, and then dispersed in absolute ethyl alcohol. The 2-3 drops of the dispersion were dripped onto a carbon-coated TEM grid. The crystalline phase and phase purity of the Pd nanoparticles and Ni@Pd particles were analyzed by X-ray diffraction (XRD) using D8 Advance X-ray diffraction (Bruker axs company, Germany) equipped with Cu-KR radiation (λ) 1.5406 (Å), employing a scanning rate of 0.02° s^{-1} in the 2θ range from 10° to 80°. X-ray photoelectron spectroscopy (XPS) was recorded on a PHI-5702, and the C1S line at 291.4 eV was used as the binding energy reference. The graphitization degree of N doped-graphene was determined by Laser Micro-Raman Spectrometer (Renishaw inVia, Renishaw plc, UK). All electrochemical measurements were performed in a three-electrode cell on an IM6e potentiastat (Zahner-Electrik, Germany) at 30°C controlled by a water-bath thermostat. A platinum foil (1.0 cm^2) and Hg/HgO (1.0 mol dm^{-3} KOH) were used as counter and reference electrodes, respectively.

3. Results and discussion

The schematic illustration for the formation of Ni@Pd/NG nanocomposite is shown in Fig. 1. Once graphite oxide was synthesized, it was dispersed thoroughly in urea solution by sonication and was heated at 180°C for 12 h. Then，it was subjected to microwave (MW) heating in a microwave oven after nickel nitrate was added. Finally the Ni/NG being added in H_2PdCl_4 solution and continuously stirred for 14 h at room temperature, well dispersed Ni@Pd nanoparticles with core/shell structure on N-doped graphene were obtained.

Fig. 2 shows typical XRD patterns of the as prepared of GO(a), NRGO(b), Pd/NG(c), Ni@Pd/NG (d) composites. All peaks can be indexed with face centered cubic (fcc) structures. The original graphite oxide sample shows a strong diffraction peak centered at $2\theta = 9.8°$, corresponding to the (001) reflection of graphene oxide, far smaller than that of pristine graphite [33] (Fig. 2(a)). After surface doped, the N-doped graphene revealed negligible C (001) peaks compared to GO (Fig. 2(b)). The weakening of the crystalline C (001) peak suggested that urea corrosion and defects resulted from nitrogen doping made the interlayer spacing larger. In addition, as seen from the XRD pattern of Fig. 2(c), the diffraction peaks at the 2θ of 40.1°, 46.5° and 68.2°can be indexed to the characteristic (111), (200) and (220) cubic crystalline structured Pd. Besides, as it is displayed in Fig. 2(d), positive shift of the Pd peaks occurs obviously on the Ni@Pd/NG comparing with the Pd/NG, indicating the Ni atoms enter into the Pd crystals which caused a very small change of the Pd crystal lattice distance. Jiang et al [34] reported that the variation of crystal lattice parameters of noble metal could obviously improve its catalytic activities. This can also be attributed to the decorating effect of the Pd atomic shell layer on the alloyed nanoparticles. The Pd particle size was calculated from all the Pd crystal plane parameters and averaged as 2.8 for Ni@Pd/NG, which are very close to the TEM results.

Raman spectroscopy is a powerfuland widely used tool for identifying graphene-based materials and detecting the doping effect of GO, such as defect structures and disordered crystal structures of carbon and carbon-heteroatoms from carbon-carbon bonds [35] Fig. 3 compared the Raman spectra of GO, NRGO and Ni@Pd/NG. All samples displayed one intense D band at 1347.27 cm^{-1} due to the indicative of the expected crystallite structure of graphite [36] and one relatively weak G band due to the optically allowed E_{2g} mode. A blue shift of the G band is usually a result of the effects of disorder and the presence of isolated short double-bond segments[37]. It is noteworthy that of the NGO (1583.03cm^{-1}, Fig. 3c) and Ni@Pd/NG composites (1578.18cm^{-1}, Fig. 3a) exhibit blue shifts compared with that of GO (Fig. 3b). It reveals that the partial N heteroatoms may be introduced on these structural sites to form substitutional N species during nitridation and can increase the numbers of structural defects on grapheme surface[38]. These indicate the electronic interaction between NRGO and Ni@Pd for electron transportation between NRGO and Ni@Pd. In addition, the intensity ratio of the D bandand G band (ID/IG) is an indication of the number of structural defects and a quantitative measure of edge plane exposure, which is most commonly being used as the level of doping and the chemical modification of graphitic carbon sample [39]. It is found that ID/IG values of Ni@Pd/NG (1.13) and NGO (1.10) are higher than that of GO (1.02), indicating the successful nitrogen doping into RGO that can induce higher concentration of structure defect [40]. Such a

View Article Online
DOI: 10.1039/C6RA06416G

higher ratio of D peak and G peak in Ni@Pd/NG is attributable to the decrease in the average size of the sp^2 domains upon the formation of nanoparticles on the graphene and the structural defects and edge plane exposure caused by nitrogen atom incorporation into the graphene layers [41].

The morphology and element distribution of Ni@Pd nanoparticles supported on NG were investigated by TEM and EDS as shown in Fig. 4. Compared with GO (Fig. 4a), the NRGO (Fig. 4b) appeared to obviously aggregate with more layers. It has been proved experimentally that the defects created by nitrogen doping act as the anchoring sites for the uniform dispersion of small metal nanoparticles homogeneously on the surface even without any additional protective reagents or surfactants in the system(Fig. 4c). The HRTEM image describing the crystalline nature of Ni@Pd nanoparticles is shown in Fig. 4d. The single crystalline Ni@Pd particles are confirmed, the lattice planes with an interlayer distance of 0.203 nm in the core are indexed to Ni (111) crystal planes, the outer layer with the lattice space of 0.224 nm corresponds to Pd (111) crystal planes. The elemental analysis by EDS proves that the Ni@Pd/graphene is composed of C, Ni and Pd (Fig. 4e, the Cu signal comes from the sample holder). The particle size distribution of Ni@Pd/NG particles derived from TEM image are a narrow diameter range from 1.5 to 4.5 nm and the average diameter is about 2.8nm (Fig. 4f). Clearly, nickel nanoparticles interacting strongly with the N-doped graphene surface plays a key role in keeping a similar and highly disperses Ni@Pd particle size on the supports. It is known that N-doped graphene tends to interact with metal species. Density functional theory

View Article Online
DOI: 10.1039/C6RA06416G

calculation was used to show that extra Ni-C bonds was formed at the interface and more electrons transferd from the interfacial C-C bonds to the Ni-C bonds [42]. It can imagine that the Ni particles were supported on N doped graphene firstly, then the Pd particle coating on the Ni core. At the same time Pd particles were fixed on the graphene because the bottom of Pd also contact with the graphene. Possibly, palladium and nickel nano-particles have strong interaction with the N doped graphene surface, which restrains the aggregation and the growth of the nanoparticles to form larger particles, resulting in the uniform distribution of these nanoparticles.

XPS were further performed to analyze the chemical compositions, oxidation states and nitrogen bonding configurations of Ni@Pd/NG catalysts. The high resolution XPS spectra of C 1s (Fig. 5a) show that there were three peaks (C-C, 283.9 eV; C-N, 285.5 eV; C=O, 287.9 eV). The peak centered at 283.9 eV can be assigned to the adventitious hydrocarbon from the defect-containing sp^2 hybridized carbon atoms present in graphitic domains, and the C-N bond (285.5 eV) is suggesting that the N was successfully doped in graphene nanosheets [43]. Moreover, the signal of the high resolution N1s peak (Fig. 5b) could be deconvoluted into three characteristic peaks corresponding to the presence of pyridinic N, pyrrolic N and quaternary N in the Ni@Pd/NG [44]. As previous reports, the pyridinic N (398.3 eV) contributed to nitrogen atoms at the edge of graphene planes that are bonded to two carbon atoms and donate one p electron to the aromatic π system, the pyridinic edge sites can also provide a stronger interaction between catalyst nanoparticles and carbon support and this reduces the agglomeration of a core-shell nanophase. pyrrolic N (399.4 eV)

View Article Online
DOI: 10.1039/C6RA06416G

referred to the N atom contributing two p-electrons to the p system due to the contribution of pyridine and pyrrol functionalities; and quaternary N (400.8 eV) was derived from the graphene layers by replacing a carbon atom within a graphene plane and contributes two p electrons to the π system [45,46].The detailed Pd_{3d} spectra of catalysts (Fig. 5c) displayed a doublet consisting of a high-energy band ($Pd3d_{3/2}$) and a low-energy band ($Pd3d_{5/2}$) at 339.98 and 334.65 eV for Ni@Pd/NG, such binding energy values are in accordance with those reported for entered into the Pd lattice and a core/shell of Ni@Pd was formed. The peaks of Ni $2p_{3/2}$ and Ni $2p_{1/2}$, which were located at around 855.5 and 873.4 eV (Fig. 5d), were assigned that nickel is composed of two surface chemical states on N doped-graphene. Remarkably, there are some extra peaks labeled as satellite peaks which are present around the expected Ni $2p_{3/2}$ and Ni $2p_{1/2}$ signals in the Ni 2p region[47].

As a highly useful technique, cyclic voltammograms (CVs) is frequently used to investigate the heterogeneous the electron transfer ability occurring on the electrode surface. Fig.6 (a) shows the cyclic voltammograms (CVs) of alcohol electro-oxidation on above prepared electrodes in 1.0 M KOH + 1.0 M ethanol solution at 303 K and electrodes at a scan rate of 50 mV s^{-1}. Two featuring well-strong anodic current peaks were observed in the CV curves of the different catalysts (Fig.6 (a)). The oxidation peak in the forward scan were reminiscent the amount of ethanol electro-oxidation process at the Pd-based electrocatalysts and consistent with the literature reports. [48, 49]

The reverse scan peak is primarily associated with the removal of carbonaceous species which are not completely oxidized in the forward scan[50]. More explicitly, the

View Article Online
DOI: 10.1039/C6RA06416G

mass activity of the ethanol oxidation in 1 mol dm^{-3} ethanol solution on Ni@Pd/NG was 3650 mA mg_{Pd}^{-1}, which is higher than that of 2435 mA mg_{Pd}^{-1} on Pd/NG and also higher than that of 1528 mA mg_{Pd}^{-1} on Pd/G electrode. The Ni@Pd/ NG electrode shows 4.5 times peak current density as high as that on Pd/C electrocatalyst at the same Pd loadings during the similar electrochemical reaction conditions. The activities of the Ni@Pd/ NG electrocatalyst were most likely a result of the particular structure of bimetallic nanodendrites and the highly surface area of N-doped graphene as support being beneficial for the uniform dispersion of the Ni@Pd nanoparticles to make them highly used for the easier mass transfer, which display mast commercial competition. When the Ni was added to form the Ni-Pd alloy, according to Zhang's report [51], the Ni would transform to $Ni(OH)_2$ in alkaline media at the reaction potential and consequently increase the coverage of OH_{ads} on Pd surface, which would ultimately accelerate the reaction rate through the Eq.:

$$Pd\text{-}(CH_3CO)_{ads} + OH^- \xrightarrow{Ni(OH)_2} Pd\text{-}CH_3COOH + e^-$$

The above results were further evidenced by comparing the electrochemical active surface area (EASA) as shown in Fig.6 (b) in the KOH solution without ethanol. As shown in 6(b), the peaks between -0.9 and -0.5 V originated from the hydrogen adsorption-desorption[52,53]. On the reverse sweep, the defined peak near -0.25 V was characteristic of the reduction of Pd oxide formed during the positive-going sweep to Pd. No other obvious characteristic peaks appear in the CV curves in the KOH solution with or without alcohol, which is consistent with the literature reports[54].

The EASA of the above catalysts were studied by CV tests from −0.70 to 0.20 V in

1.0 mol L^{-1} KOH at a scan rate of 50 mV s^{-1}, and were calculated based on the PdO reduction peak adapting, and the assumption of 212 uC cm^{-2} of the electrode surface [55]. They are 158.7 m^2 g^{-1}, 103.6 m^2 g^{-1}, 85.8 m^2 g^{-1} and 59.4 m^2 g^{-1} for the Ni@Pd/ NG, Pd/NG, Pd/G and Pd/C, respectively. The EASA on Ni@Pd/ NG is 2.7 times higher than that on Pd/C. The largest EASAs of Ni@Pd/ NG catalyst is mainly due to the replacement of Pd active sites on the surface by N-doped active center, also due to its high specific surface area for shell structure. Furthermore, theoretical study has shown that nitrogen-doped reduced graphene oxide leads to a higher positive charge on a carbon atom adjacent to the nitrogen atoms, and a positive shift of Fermi energy at the apex of the Brillouin zone of graphene readily attracts electrons from the anode to facilitate the ethanol oxidation process [56]. Moreover, the Ni@Pd/ NG has about 40 mV negative onset potential than that on Pd/NG. The negative shift indicated that ethanol was more easily oxidized by Ni@Pd/ NG, which was evidence that the core-shell structure could tremendously improve the kinetics of the ethanol electro-oxidation[57]. The results further indicated that the Ni@Pd significantly improved the activity and the output when used in fuel cells.

The stabilities of the Ni@Pd/ NG and Pd/ G electrodes for ethanol oxidation are shown in Fig.7. The dotted lines are the cycling difference from the 1st cycle to the 3,000th cycle. It is clear that the EASA of the Pd/ G electrodes reduced 17.6% from 85.8 m^2 g^{-1} to 70.7 m^2 g^{-1} for ethanol oxidation after the 3,000th cycle. However, the EASA of the Ni@Pd/ NG reduced 8.9 % from 158.7 m^2 g^{-1} to 144.6 m^2 g^{-1}. It is evident that the Ni@Pd/ NG electrocatalyst has a higher stability than the Pd/ G. The

View Article Online
DOI: 10.1039/C6RA06416G

promoted electrochemical stability may be due to the stronger interaction force between Ni@Pd and N doped-graphene than the force between Pd and graphene.

The improved mass transfer property of the Ni@Pd/ NG electrocatalyst was evidenced by performing various scan rates for ethanol oxidation (Fig. 8). The deflection from the linear line of the data at lower scan rates in the relationship of peak current density and square root of scan rate on electrode indicates the improvement in the mass transfer. The straight line appears over the scan rate of 49 mV s^{-1} on Ni@Pd/ NG comparing with Pd/G (20 mV s^{-1}), indicating N doped-graphene improved mass transfer, however, it shows a straight line at any scan rate on Pd/C electrode, indicating the concentration polarization.

The chronoamperometric curves on the three electrodes at a fixed potential of -0.18V were shown in Fig. 9. As can be seen that the initial current densities decrease rapidly for all the three catalysts owing to the formation of reactive intermediates such as CO_{ads}, CH_3COOH_{ads} and CH_3CHO_{ads} during the electrochemical reaction process[58], but the Ni@Pd/NG shows the highest initial and highest steady-state current density than the Pd/NG and PD/C, indicating that the Ni@Pd/NG hybrid possessed a good catalytic durability and excellent catalytic activity.

The data of CVs and chronoamperometric measurement suggested that the Ni@Pd/NG exhibited an enhanced catalytic activity and good stability for ethanol electro-oxidation. The superior electrocatalytic performance of the proposed catalyst (Ni@Pd/NG) could be attributed to the following factors. Firstly, it is approved that the catalyst surface structure strongly affected catalytic activity. The core/shell

View Article Online
DOI: 10.1039/C6RA06416G

structure catalysts have different intermetallic surface structure or the downshift in d-band energy center of the noble metal, which will certainly affect the catalytic activity. Researchers called it electric “ligand effect” that between the two metal layers of the core/shell catalyst, which could promote desorption of the toxic intermediate products such as CO from the noble metal, and consequently improve the anodic catalyst activity and stability [59,60]. Secondly, the N doped on the graphene sheets could not only help the formation of small, highly concentrated and uniformly dispersed Ni@Pd nanoparticles, but also the doped N, acted as a secondary catalyst increasing more catalytic activity center and the rapidly removal of intermediate poisoning species. In addition, the Ni@Pd/NG was possessed of a larger EASA compared with the other electrocatalysts because of more catalytic activity center of N-doped graphene, a narrower size distribution, more uniform distribution and more perfect crystal structure on N-doped graphene than those of other as-prepared composites.

4. Conclusions

In summary, Ni@Pd/NG nanocomposites have been successfully fabricated through an environmentally friendly two step strategy, and the catalytic properties toward the ethanol oxidation are investigated. As a new catalyst, the Ni@Pd/NG exhibits better kinetics, large specific surface areas, higher tolerance and electrochemical stability than the other catalysts for ethanol electro-oxidation in

View Article Online
DOI: 10.1039/C6RA06416G

DEFCs, which was correlated with the core shell architecture, nitrogen doping of graphene, and the synergistic effects between Ni and Pd. Importantly, the Ni cores of the Ni@Pd NPs reduced the consumption of Pd, N-doped grapheme had a large specific surface area and more active site. This remarkable improvement of the electrocatalytic performance may strongly provides new insights into the other graphene-based metallic systems and prepare good electrocatalyst materials in alcohol oxidation for fuel cells.

Acknowledgements

This work was supported by the financial supports from Natural Science Foundations of Jiangsu (BK20140531), Zhenjiang Industry Supporting Plan (GY2014040), China Postdoctoral Science Foundation (2015M570410) and Research Foundation for Talented Scholars of Jiangsu University (14JDG187); Dr. Suci Meng thanks National Natural Science Foundation of China (21103073)

References

[1] J. Wu and H. Yang, *Acc. Chem. Res.* 2013, **46**,1848.

[2] M. K. Debe, *Nature*, 2012,**486**, 43.

[3] Z.X.Yan, M.M. Zhang, J.M. Xie, J.J. Zhu and P.K. Shen, *Appl. Catal. B-Environ.* 2015, **165**, 636.

[4] D.P. He, K. Cheng, H.G. Li, T. Peng, F. Xu, S.C. Mu and M. Pan, *Langmuir*, 2012, **28**, 3979.

[5] Z. X.Yan, M. Cai and P. K.Shen, *J. Mater. Chem.*, 2012, **22**, 2133.

[6] S.H. Xu,Z.F. Li , Y.F Ji, S.W. Wang, X.Y.Yin and Y.X. Wang, *Int. J. Hydrogen. Energ.*, 2014, **39**, 20171.

[7] M.M.Zhang, J.M.Xie, Q.Sun, Z.X.Yan, M.Chen and J.J.Jing, *Int. J. Hydrogen Energy.* 2013,**38**,16402.

[8] M.M.Zhang, J.M.Xie, Q.Sun, Z.X.Yan, M.Chen and J.J.Jing, A.M. S. Hossain, *Electrochimica Acta* 2013,**111**,855.

[9] Z.X.Yan, M.M.Zhang, J.M.Xie and P.K.Shen, *J. Power Sources,* 2013, **243**,336.

[10] S.Y. Wang, D.S. Yu, L.M. Dai, *J Am Chem Soc*, 2011,**133**, 5182.

[11] K. Tedsree, C. W. A. Chan, S. Jones, Q. Cuan, W. K. Li, X. Q. Gong and S. C. E. Tsang, *Science* , 2011,**332**, 224.

[12] H. Yin, H. Tang, D. Wang, Y. Gao and Z. Tang, *ACS Nano*, 2012,**6**, 8288.

[13] A. Alayoglu, A.U. Nilekar, M. Mavrikakis and B. Eichhorn, *Nat. Mater.*, 2008,**7** ,333.

[14] M.M.Zhang, Y. Li, Z.X.Yan, J.J. Jing, J.M.Xie and M. Chen. *Electrochimica Acta* , 2015,158, 81.

[15] S.H.Zhou, B.Varughese, B.Eichhorn, G.Jackson and K.McIlwrath, *Angew. Chem. Int. Ed.,* 2005, **44**, 4539.

[16] M.M.Zhang, Z.X.Yan, Q. Sun, J.M Xie and J.J Jing, *New J. Chem.* 2012,**36**,2533.

[17] O. Metin, S.F. Ho, C. Alp, H. Can, M.N. Mankin, M.S. Gultekin, M. Chi and S. Sun, *Nano Res.* 2013,**6**, 10.

[18] Z.X.Yan, J.M. Xie, P.KShen, M.M.Zhang, Y. Zhang and M.Chen, *Electochimica Acta*, 2013,**108**,644.

[19] Z.X.Yan, W.Wei, J.M.Xie, S.C.Meng, X.M. Lü and J.J. Zhu, *J. Power Sources* ,2013,**222**, 218.

View Article Online
DOI: 10.1039/C6RA06416G

[20] Y.H. Lu, M. Zhou, C. Zhang and Y.P. Feng, *J.Phy.Chem. C* 2009,**113**,20156.

[21] X. M. Chen, G. H. Wu, J.M. Chen, X.Chen, Z.X. Xie and X.R. Wang, *J. Am. Chem. Soc.,* 2011, **133**,3693.

[22] S. Li, H. Yang, Z. Dong, S. Guo, J. Zhao, G. Gou, R. Ren, J. Huang, J. Jin and J. Ma, *Catal. Sci. Technol.,* 2013,**3**, 2303.

[23] D. He, K. Cheng, H. Li, T. Peng, F. Xu, S. Mu and M. Pan, *Langmuir,* 2012,**28**, 3979.

[24] D.P. He, Y.L. Jiang, H.F.Lv, M. Pan and S.C.Mu. *Appl. Catal. B-Environ.* 2013,**132**,379.

[25] L.S. Zhang, X.Q. Liang, W.G. Song and Z.Y. Wu, *Phys. Chem. Chem. Phys.* 2010,**12**, 12055.

[26] H.L. Guo, P. Su, X. Kang and S.K. Ning, *J. Mater. Chem. A*, 2013, **1,** 2248.

[27] L. Sun, L. Wang, C. Tian, T. Tan, Y. Xie, K. Shi, M. Li and H. Fu, *RSC Adv.*, 2012, **2** ,4498.

[28] H. M.Jeong, J. W.Lee, W. H.Shin, Y. J.Choi, H. J.Shin, J. K.Kang and J. W. Choi, *Nano Lett.*, 2011, **11**,2472.

[29] Z. S.Wu, A.Winter, L.Chen, Y.Sun, A.Turchanin, X.L.Feng and Müllen, *Adv. Mater.*, 2012, **24**, 5130.

[30] S.Y. Yang, K.H. Chang and Y.L .Huang, *Electrochem. Commun.*, 2012,**14**,39.

[31] A. Tegou, S. Papadimitriou, I. Mintsouli, S. Armyanov, E. Valova, G. Kokkinidis and S. Sotiropoulos, *Catalysis Today*, 2011,**170**,126.

[32] M.M.Zhang, Z.X.Yan, Y. Li, J.J.Jing and J.M. Xie. *Electrochimica Acta*, 2015,**161**,48.

View Article Online
DOI: 10.1039/C6RA06416G

[33] B. Zhao, P. Liu, Y. Jiang and D. Pan, *J Power Sources*, 2012,**198**,423.

[34] .A. Wu, S.W. Ong, H.C. Kang and E.S. Tok, *J. Phys. Chem. C*, 2010,**114,**21252.

[35] H.B. Wang, T. Maiyalagan and X. Wang, *ACS Catal.,* 2012,**2**,781.

[36] Z.H.Sheng, L. Shao, J. J.Chen, W.J. Bao, F.B. Wang and X.H. Xia, *ACS Nano*, 2011, **5**, 4350.

[37] E. F. Antunes, A. O. Lobo, E. J. Corat, V. J. Trava Airoldi, A. A. Martin and C. Veríssimo, *Carbon*, 2006, 44, 2202.

[38] O.S. Kwon, S.J. Park, J.Y. Hong, A.R. Han, J.S. Lee, J.H. Oh and J. Jang, *ACS Nano*, 2012, **6**,1486.

[39] Y.J.Zhang, K. Fugane, T. Mori, L. Niu and J.H. Ye, *J. Mater. Chem.,* 2012,**22**,6575.

[40] W.X. Wang, S.H. Liang, T. Yu, D.H. Li, Y.B. Li and X.F. Han, *J. Appl. Phy.* 2011,**109**,C501.

[41] D.S. Geng, S.L. Yang, Y. Zhang, J.L Yang, J. Liu, R.Y. Li, T.K. Sham, X.L. Sun, S .Y. Ye and S. Knights, *Appl. Surf. Sci*., 2011, **257**,9193.

[42] M.T. Zhao, W.Xiao, H.J.Zhang and K.Cho, *Phys. Chem. Chem. Phys.*, 2011, **13**, 11657.

[43] H.J. Yin, H.J .Tang, D. Wang, Y. Gao and Z.Y. Tang, *ACS Nano*, 2012,**6**,8288.

[44] E. Yoo, J. Nakamura and H.S. Zhou, *Energy Environ. Sci.*, 2012, **5**, 6928.

[45] L. Sun, L. Wang, C. Tian, T. Tan, Y. Xie, K. Shi, M. Li and H. Fu, *RSC Adv.*, 2012,**2**,4498.

[46] S.Maldonado, S.Morin and K. J. Stevenson, *Carbon*, 2006,**44**, 1429.

[47] H. Chen, L.F. Hu, M. Chen, Y. Yan, and L.M. Wu. *Adv. Funct. Mater.* 2014, 24, 934.

[48] S. Guo, S. Dong, E. Wang, *Adv. Mater.* 2010, 22, 1269.

[49] Q. Tan, C. Du, Y. Sun, G. Yin, Y. Gao, *J. Mater. Chem. A,* 2014, 2, 1429.

[50] Z. Bai, P. Xu, S. Chao, H. Yan, Q. Cui, L. Niu, L. Yang, J. Qiao, *Catal. Sci. Technol*. 2013, 3, 2843.

[51] Z.Y. Zhang, L. Xin, K. Sun and W.Z. Li, *Int. J. Hydrogen Energy*, 2011,**36**,12686.

[52] X. Chen, Z. Cai, X. Chen, M. Oyama, *J. Mater. Chem. A*, 2014, 2, 315.

[53] V. Bambagioni, C. Bianchini, Y. Chen, J. Filippi, P. Fornasiero, M. Innocenti, A. Lavacchi, A. Marchionni, W. Oberhauser, F. Vizza, *ChemSusChem*, 2012, 5 1266.

[54] H. Yang, H. Wang, H. Li, S. Ji, M.W. Davids, R. Wang, *J. Power Sources* , 2014,260, 12.

[55] S.Y. Wang, D.S. Yu, L.M. Dai, D.W. Chang and J.B. Baek, *ACS Nano,*2011, **5,**6202.

[56] S.U. Lee, R.V. Belosludov, H. Mizuseki, Y. Kawazoe, *Small*, 2009,**5**,1769.

[57] H.T. Zheng, Y. Li, S. Chen, P.K. Shen, *J. Power Sources*, 2006, 163, 371.

[58]Y.B. He, G.R. Li, Z.L. Wang, Y.N. Ou and Y.X. Tong, *J. Phys. Chem. C*, 2010, 114, 19175.

[59] A.C. Garcia, V.A. Paganin and E.A.Ticianelli *Electrochimica Acta,* 2008, **53**,4309.

[60] S. Papadimitriou, A. Tegou, E. Pavlidou, G. Kokkinidis and S. Sotiropoulos, *Electrochim. Acta*, 2007, **52**, 6254.

View Article Online
DOI: 10.1039/C6RA06416G

Figure captions

Fig.1 Schematic diagram of the synthesis of Ni@Pd nanocatalysts on N doped graphene.

Fig.2 shows typical XRD patterns of the as prepared of GO(a), NRGO(b), Pd/NG(c), Ni@Pd/NG (d) composites.

Fig.3 Raman spectra of a (Ni@Pd/NG), b (GO), and c (NRGO)

Fig.4 TEM images of GO (a), NRGO (b), Ni@Pd/NG (c) ,HRTEM images of Ni@Pd/NG (d), EDS spectrum of Ni@Pd/NG (e) and Size distribution of mental particles of Ni@Pd/NG derived from TEM images (f).

Fig.5 XPS spectra of (a) C 1s, (b) N 1s, (c) Pd 3d and (d) Ni 2p of the sample Ni@Pd/NG.

Fig.6 (a) cyclic voltammograms of ethanol oxidation on Ni@Pd/NG, Pd/NG, Pd/G and Pd/C electrodes and (b) cyclic voltammograms of Ni@Pd/NG, Pd/NG, Pd/G and Pd/C electrodes in 1.0 mol dm^{-3} KOH solution at 303 K, scan rate: 50 mV s^{-1}.

Fig. 7 (A) the cyclic voltammograms of the Ni@Pd/NG electrocatalysts and (B) the cyclic voltammograms on Pd/G in 1.0 mol dm^{-3} KOH solution at 303 K, scan rate: 50 mV s^{-1}. The dotted line shows the difference from the 1st cycle to the 3000th cycle.

Fig. 8 plots of the peak current density against the square root of the scan rate for Ni@Pd/NG, Pd/G and Pd/C electrodes in 1.0 mol dm^{-3} ethanol/1.0 mol dm^{-3} KOH solution, 303 K.

Fig. 9. Chronoamperometric curves of Ni@Pd/NG, Pd/NG and Pd/C at -0.18 V (vs SCE) in 1.0 M KOH + 1.0 M ethanol solution.

View Article Online
DOI: 10.1039/C6RA06416G

Fig.1. Schematic diagram of the synthesis of Ni@Pd nanocatalysts on N doped graphene.

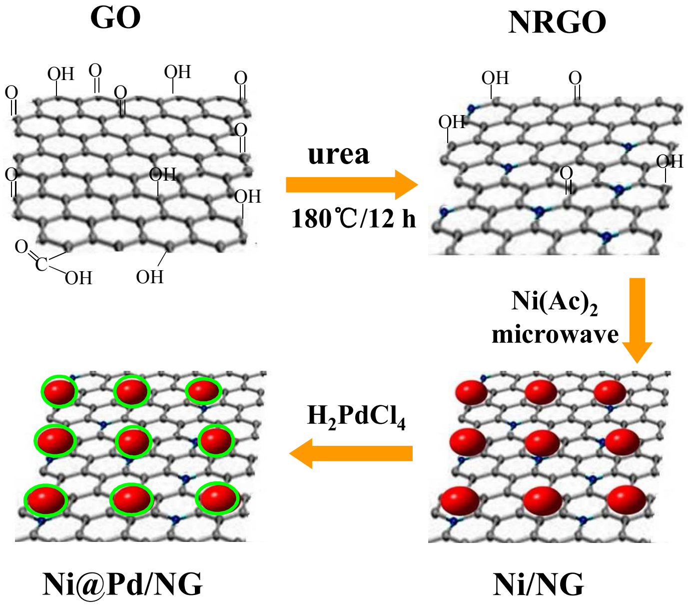

View Article Online
DOI: 10.1039/C6RA06416G

Fig.2 shows typical XRD patterns of the as prepared of GO(a), NRGO(b), Pd/NG(c), Ni@Pd/NG (d) composites.

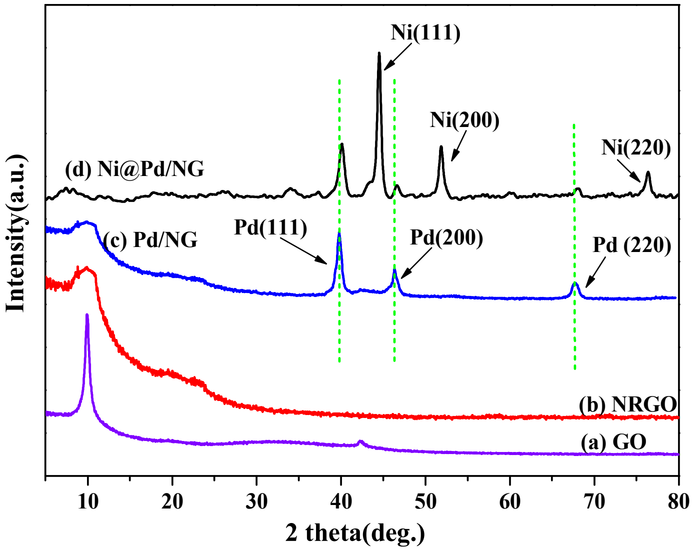

View Article Online
DOI: 10.1039/C6RA06416G

Fig.3 Raman spectra of a (Ni@Pd/NG), b (GO), and c (NRGO)

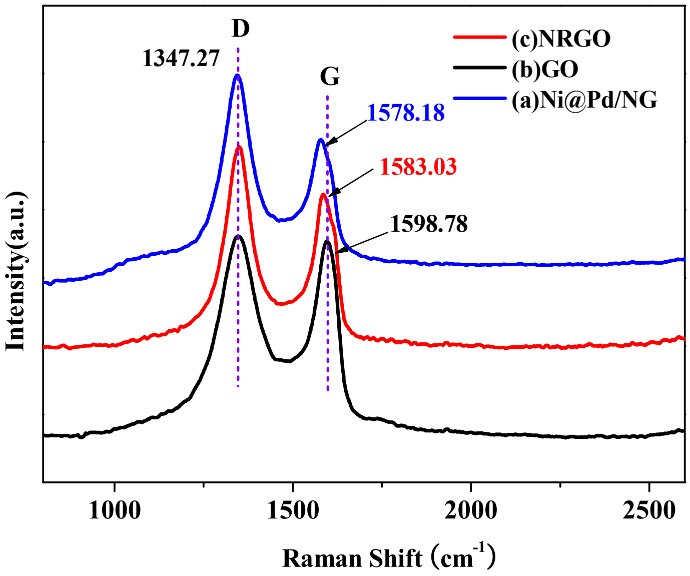

View Article Online
DOI: 10.1039/C6RA06416G

Fig.4 TEM images of GO (a), NRGO (b), Ni@Pd/NG (c) ,HRTEM images of Ni@Pd/NG (d), EDS spectrum of Ni@Pd/NG (e) and Size distribution of mental particles of Ni@Pd/NG derived from TEM images (f).

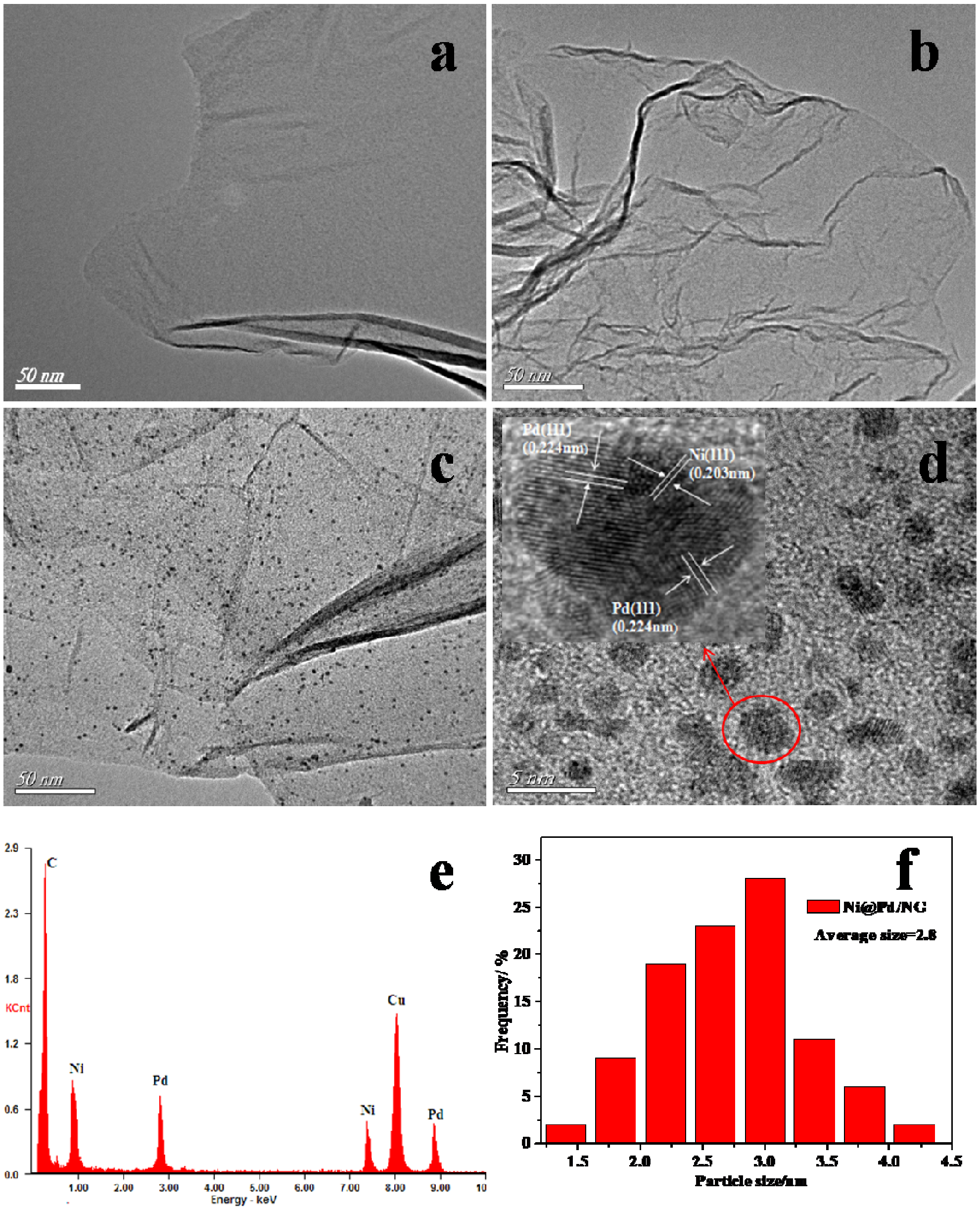

View Article Online
DOI: 10.1039/C6RA06416G

Fig.5 XPS spectra of (a) C 1s, (b) N 1s, (c) Pd 3d and (d) Ni 2p of the sample Ni@Pd/NG.

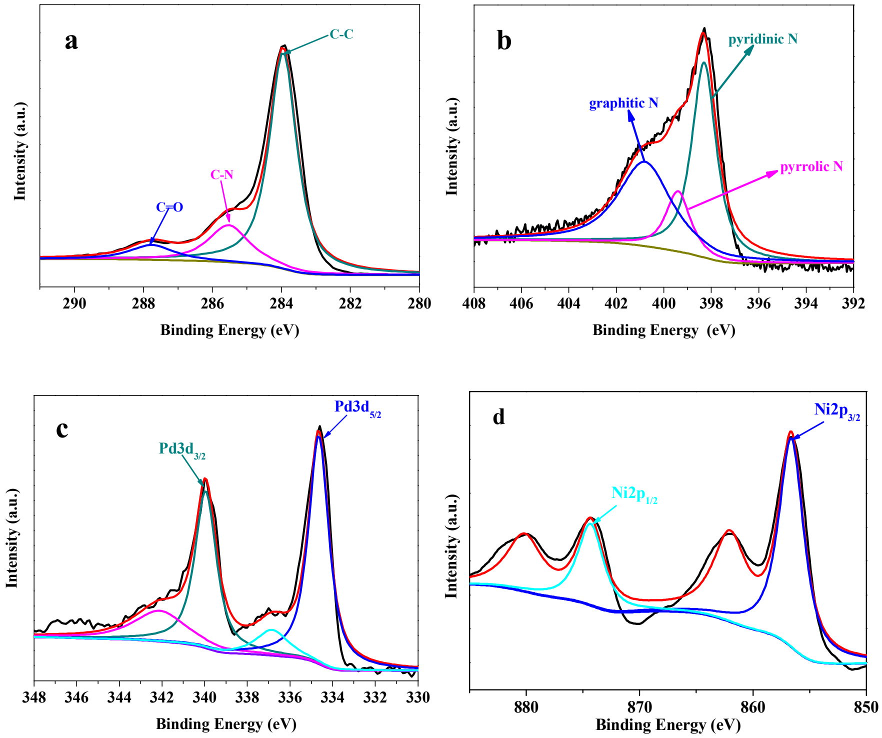

View Article Online
DOI: 10.1039/C6RA06416G

Fig.6 (a) cyclic voltammograms of ethanol oxidation on Ni@Pd/NG, Pd/NG, Pd/G and Pd/C electrodes and (b) cyclic voltammograms of Ni@Pd/NG, Pd/NG, Pd/G and Pd/C electrodes in 1.0 mol dm^{-3} KOH solution at 303 K, scan rate: 50 mV s^{-1}.

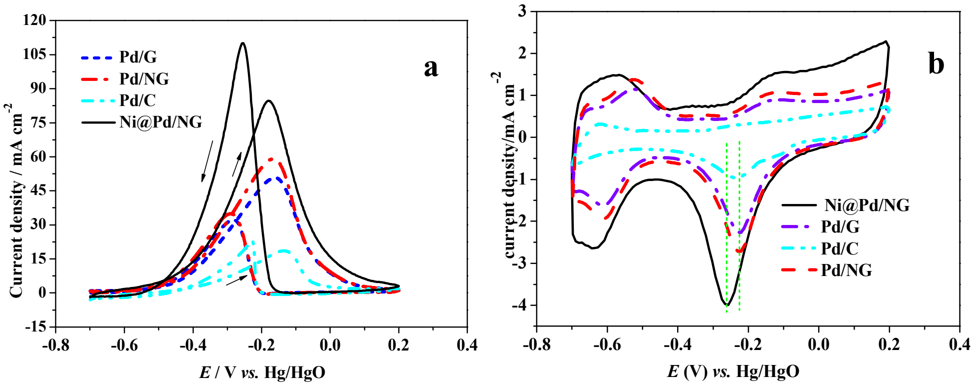

View Article Online
DOI: 10.1039/C6RA06416G

Fig. 7 (A) the cyclic voltammograms of the Ni@Pd/NG electrocatalysts and (B) the cyclic voltammograms on Pd/G in 1.0 mol dm^{-3} KOH solution at 303 K, scan rate: 50 mV s^{-1}. The dotted line shows the difference from the 1st cycle to the 3000th cycle.

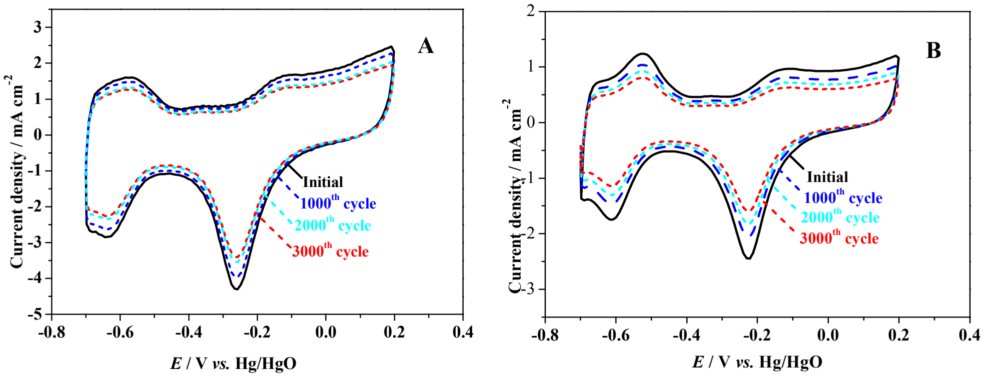

View Article Online
DOI: 10.1039/C6RA06416G

Fig. 8 plots of the peak current density against the square root of the scan rate for Ni@Pd/NG, Pd/G and Pd/C electrodes in 1.0 mol dm^{-3} ethanol/1.0 mol dm^{-3} KOH solution, 303 K.

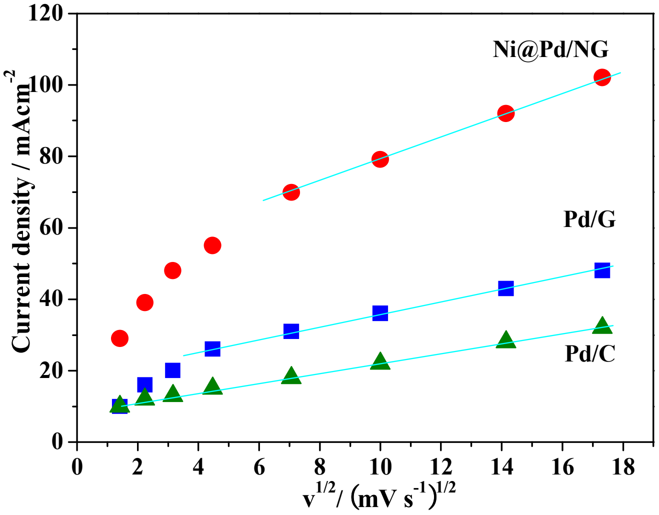

View Article Online
DOI: 10.1039/C6RA06416G

Fig. 9. Chronoamperometric curves of Ni@Pd/NG, Pd/NG and Pd/C at -0.18 V (vs SCE) in 1.0 M KOH + 1.0 M ethanol solution.